ACS APPLIED MATERIALS & INTERFACES

Research Article

www.acsami.org

Layer-Dependent Optical Conductivity in Atomic Thin WS_2 by Reflection Contrast Spectroscopy

Pramoda K. Nayak, Chao-Hui Yeh, Yu-Chen Chen, and Po-Wen Chiu*

Department of Electrical Engineering, National Tsing Hua University, Hsinchu 30013, Taiwan

Supporting Information

ABSTRACT: Optical conductivity, which originates from the interband transition due to electron−phonon interaction, is one of the powerful tools used for studying the electronic states in layered transition metal dichalcogenides (TMDCs). Here, we report for the first time the optical conductivity of WS_2, one of the emerging classes of TMDCs, prepared directly on SiO_2/Si substrate using reflection contrast spectroscopy. The measured optical conductivity at direct excitonic transition point K of the Brillouin zone for monolayer WS_2 shows a value of 0.37 $e^2/\pi\hbar$ in the visible range of the energy spectrum. Our results reveal that the optical conductivity of WS_2 layers is frequency-dependent and show additional features in the conductivity spectra for bilayer to bulk counterparts, signifying a transition from direct band gap to indirect band gap with the evolution of layer numbers as predicted by our calculations.

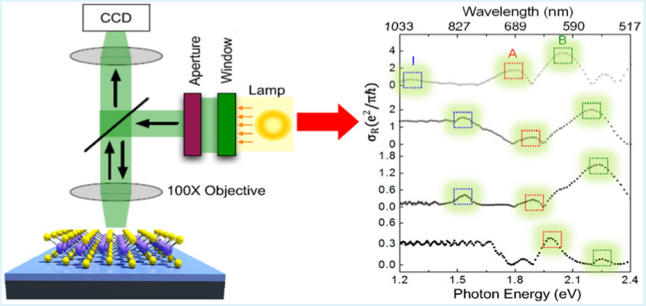

KEYWORDS: *optical conductivity, WS_2, transition metal dichalcogenides, reflection contrast spectroscopy, semiconductors*

1. INTRODUCTION

Layered transition metal dichalcogenides (TMDCs) with chemical formula MX_2 (M = W, Mo, and so on; X = S, Se, or Te) have gained a great deal of attention due to their fascinating thickness-dependent material and physical properties.[1−6] Most of the TMDCs possess a sizable band gap in a technologically interesting range of 1−3 eV,[7−11] which paves the way to consider these materials for new generation field−effect transistors, sensors, and optoelectronic devices including valleytronics.[12,13] WS_2 is one of the emerging classes of TMDCs and is formed by stacking atomic layers of S−W−S in a sandwich configuration. The crystal structure belongs to hexagonal *P*63/*mmc* space group with lattice parameters a = 3.153 Å and c = 12.323 Å.[14] The electronic states of WS_2 exhibit a strong interlayer coupling and undergo transitions from indirect band gap (in bulk) to direct band gap (in a monolayer)[15−17] when the number of layers decrease, in analogy to MoS_2 and some of other TMDCs. For monolayer WS_2, a direct gap exists at the K points of the Brillouin zone between the spin−orbit split valence band and the doubly degenerate conduction band, whereas for bulk WS_2, an indirect gap forms between a local conduction band minimum at a midpoint between Γ and K and the valence band maximum at the Γ point.[10]

It is very interesting to investigate its unique optical responses, including photoluminescence (PL), optical absorption, and photoconductivity, in order to understand the band structure of this material for practical device performance. Although the above optical properties have been intensively studied for graphene,[18−20] they are unexplored for most of the TMDCs. Recently, Gutiérrez et al.[21] reported extraordinary room-temperature PL in triangular WS_2 monolayers. Indirect-to-direct gap crossover has been demonstrated by PL and optical absorption spectra of WS_2 when scaling down from multilayer to monolayer.[5] Optical conductivity, which is defined as the transport of photons in a material, is one of the powerful tools for studying the electronic states for TMDCs.[9] It originates from the interband transition due to electron−phonon interaction. When a material absorbs a photon, the produced electrons and holes propagate with the same but opposite velocities, called band nesting.[22] In two-dimensional materials, the band nesting results in a divergence of the joint density of states, leading to very high optical conductivity. So far, the study of optical conductivity of WS_2 has been limited to theoretical prediction only,[22] and no experimental demonstration has been reported yet.

In the present work, we have synthesized mono- to few-layer triangular WS_2 micro platelets via sulfurization of predeposited ultrathin WO_3 films on SiO_2/Si wafers. We measured the optical conductivity of WS_2 platelets in the visible to near-infrared region determined by reflection contrast spectroscopy. Our results show that optical conductivity is frequency-dependent and show additional peaks in conductivity spectra during transition from direct band gap (monolayer) toward indirect band gap (two or more layers), consistent with the theoretical prediction.

Received: June 19, 2014
Accepted: August 25, 2014
Published: August 25, 2014

   dx.doi.org/10.1021/am5039483 | ACS Appl. Mater. Interfaces 2014, 6, 16020−16026

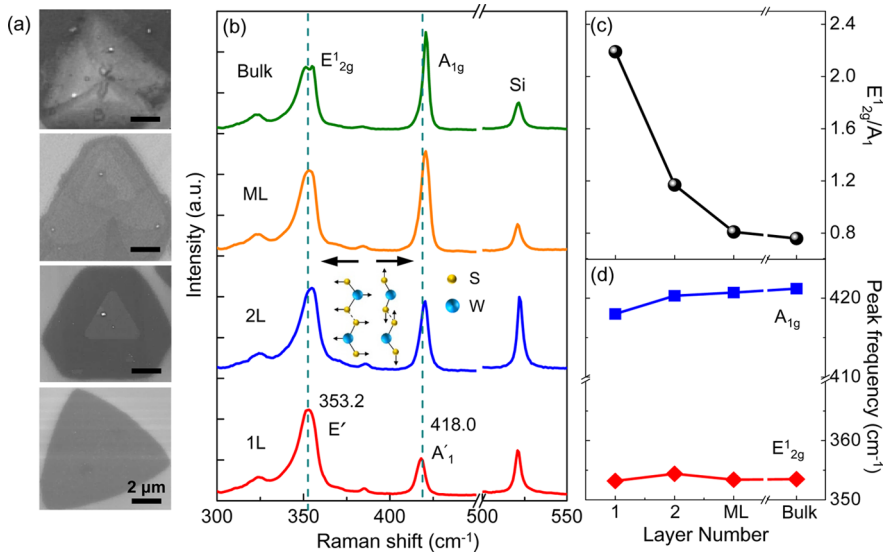

Figure 1. (a) SEM images and (b) Raman characterization of WS_2 layers directly grown on SiO_2/Si substrate using 514.5 nm excitation wavelength. E^1_{2g} and A_{1g} phonon modes along with Si peak positions are labeled. For monolayer WS_2, these phonon modes are regarded as E' and A'_1.[29] (c) The ratio of E^1_{2g}/A_{1g} peak intensity as a function of number of layers; (d) the peak positions of E^1_{2g} and A_{1g} as a function of film thickness in WS_2.

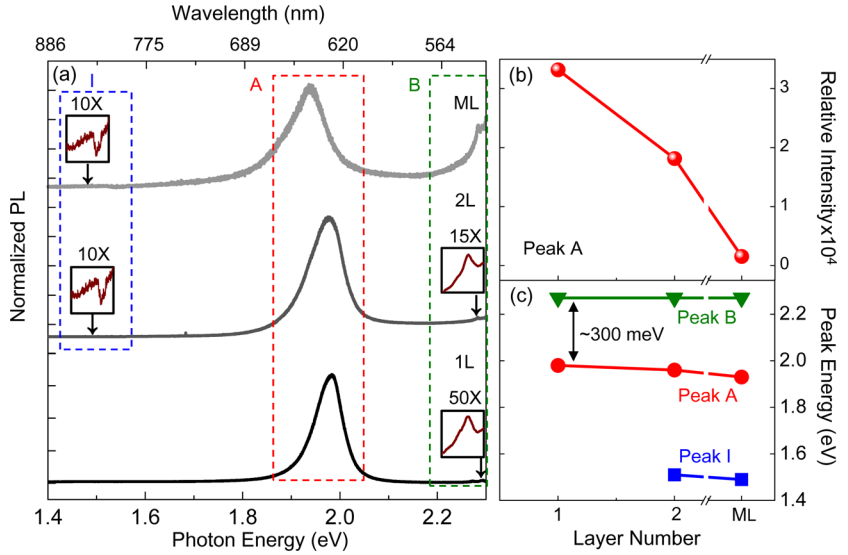

Figure 2. (a) Normalized PL spectra as a function of photon energy for WS_2 films including monolayer, bilayer, and multilayer. A and B peaks are the direct gap transitions from the split valence band edge to the conduction band edge at K points. Luminescence from indirect gap inter band transitions is labeled I. Spectra in the zoom windows have been multiplied by a factor as indicated for clarity. (b) The relative PL intensity of peak A as a function of film thickness. (c) The peak energy of A, B, and I transitions as a function of layer number. The difference in peaks A and B shows a nearly constant energy of ~300 meV, which corresponds to splitting of the valence band edge.

2. RESULTS AND DISCUSSION

2.1. Surface Morphology. Figure 1a shows the scanning electron microscopy (SEM) images of as-grown WS_2 islands on SiO_2/Si substrate including monolayer, bilayer, multilayer (3–4 layers), and bulk grains. Other detailed SEM images of the WS_2 platelets grown by chemical vapor deposition (CVD) are provided in Figure S1 (Supporting Information). The monolayer islands have monoclinic contrast throughout the grain[23] and correspond to the earliest stages of growth. The regions with slightly higher contrast in the island interiors indicate the nucleation of a second layer. Further increase of contrasts in the interior of islands corresponds to multilayer or bulk WS_2. The number of layers was confirmed by atomic force microscopy in a noncontact mode (Figure S2, Supporting Information). Once the monolayer triangular island is formed to a certain size, the second layer starts nucleating from the center and grows outward. Lateral growth could eventually result in the coalescence and merge of neighboring islands of different crystalline orientations and a large variety of island morphologies like tetragon, hexagon and so on.[21]

2.2. Raman Spectroscopy. Raman spectroscopy is a fast, nondestructive, and unambiguous way to identify the thickness of layered materials including graphene[24] and TMDCs.[25−27] Room-temperature Raman spectra of monolayer to bulk WS_2 islands acquired using 514.5 nm excitation are shown in Figure 1b in the range of 300−550 cm^{-1}. Two prominent Raman peaks observed at ~350 and ~420 cm^{-1} can be assigned to two optical phonon modes, E^1_{2g} and A_{1g}, respectively.[28] The E^1_{2g}

dx.doi.org/10.1021/am5039483 | ACS Appl. Mater. Interfaces 2014, 6, 16020−16026

represents an in-plane optical mode, while A_{1g} corresponds to out-of-plane vibrations of the sulfur atoms as shown in Figure 1b inset. In the case of monolayer WS_2, these peaks at 353.2 and 418.0 cm^{-1} are assigned to E' and A_1' phonon modes, respectively, according to Zhang et al.,[29] where interlayer interaction is completely absent. The evolution of WS_2 layer numbers can be visualized from the ratio of E^1_{2g}/A_{1g} peak intensity as shown in Figure 1c. The ratio of E^1_{2g}/A_{1g} is maximum (~2.2) for monolayer and decreases to a minimum value of ~0.8 for bulk WS_2. Similar variation in peak intensity has been observed by Gutiérrez et al.[21] for WS_2 and by Lee et al.[25] for MoS_2, when the number of layers scaled down to monolayer. The frequency of A_{1g} phonon monotonically increases with an increase in the number of layers (Figure1d) due to the decreasing interlayer interaction.[25,27] The van der Waals interaction between layers in TMDCs stiffens the lattice, resulting in the softening of the A_{1g} mode. On the contrary, the E^1_{2g} phonon mode undergoes mostly a red shift with increasing number of layers, consistent with previous reports for WS_2[21] and MoS_2.[25] This might be caused by stronger dielectric screening of the long-range Coulomb interactions between the effective charges in thicker WS_2 samples.[30] Additional peaks in the Raman spectra correspond to multiphonon combinations of these primary modes.

2.3. Photoluminescence. It is predicted that WS_2 undergoes a transition from an indirect band gap of ~1.2−1.4 eV in multilayer and bulk forms to a direct band gap of ~1.9−2.01 eV in monolayer form.[15,16,31] PL measurements on our WS_2 films show clear evidence of this transition as shown in Figure 2. Monolayer WS_2 exhibits an intense PL peak at 625 nm (~1.98 eV) corresponding to the direct excitonic transition at K point,[32] whereas the emission intensity is red-shifted and dramatically reduced to almost half and 2 orders of magnitude lower for bilayer and multilayer, respectively (Figure 2b) due to an indirect band gap transition. Besides the prominent extitonic transition peak A, a weak PL peak labeled as B is observed at higher energy for all thicknesses of WS_2 films. These two exitonic peaks A and B are the direct gap transitions from the split valence band edges $\nu1$ and $\nu2$ to the conduction band edge c1 at the K point.[9] The position of peak B is almost constant at 546 nm (~2.27 eV), but the intensity increases with thickness. It should be noted that similar peak B appeared in multilayers of MoS_2[9] is absent in its monolayer form, while it is present in monolayer WS_2 reported by Zhao et al.,[5] Zeng et al.,[32] and the present work. The discrepancy in the results may be due to the weak excitonic effect that arises from different laser excitations. As shown in Figure 2c, the energy difference between the A and B peaks for monolayer WS_2, (~300 meV) is an indication of the spin−orbital interaction strength and slightly increases for an addition of extra layers due to interlayer hopping in addition to spin−orbital coupling.[33] This energy difference is slightly less than ~400 meV, as reported by Zhao et al.[5] and Zeng et al.,[32] and is presumably due to strong substrate interaction between SiO_2 and the first WS_2 layer.

In addition to excitonic transition peaks A and B, another peak at a longer wavelength, labeled I, was observed for bilayer. It shifts toward a lower energy (Figure 2c) when the number of layers increases, as shown in the middle and upper panel of Figure 2a. It originates form indirect band gap transition. Similar behavior has also been observed in the PL measurements of WS_2 layers on sapphire substrate.[34] With an increase in the number of layers, the indirect transition between the local minimum of the conduction band between K and Γ point and local maximum of the valence band at the Γ point marked, as indicated by an arrow in Figure S3 (Supporting Information), decreases in energy. Hence, competition arises from the indirect transition between these two electronic states with that of direct transition at the K point, which dramatically reduces the PL quantum efficiency and gives rise to a novel feature at longer wavelengths associated with the indirect transition for bilayer and multilayer WS_2.[5,21]

It should be noted that the indirect gap emission peak is virtually absent in the monolayer emission spectrum, indicating that it is a pure direct band gap semiconductor. This observation, along with the distinctly strong emission of monolayer, is in good agreement with the calculated results[35,36] and the recent experimental findings.[32]

2.4. Optical Conductivity. Optical conductivity, $\sigma(\omega)$, provides a deep understanding of the band structure properties of TMDCs and can be extracted using a simple technique called reflection contrast spectroscopy.[37,38] The advantages of contrast spectroscopy over absorption measurement[39] is that this measurement can be performed on any substrates with better spatial resolution on the micrometer scale[40] and does not require suspended samples. In principle, it is actually a quantitative representation of our observation based on the sensitivity to the contrast and can be given by[38,41]

$$C_R = 1 - \frac{R_W}{R_0} \tag{1}$$

Where C_R is the contrast spectra and, R_0 and R_W are the reflection spectra from the SiO_2/Si substrate and the WS_2 layers, respectively. The light reflectance (R_W) and transmittance (T_W) of bare WS_2 can be deduced using Maxwell's equations under normal light incidence for two-dimensional sheets:[42]

$$T_W = \frac{1}{|1+\beta|^2} \tag{2}$$

$$R_W = \frac{1}{|1+\beta^{-1}|^2} \tag{3}$$

Where $\beta = c\mu_0\sigma(\omega)/2$ is the absorption coefficient with typical value of 188.4 $\sigma(\omega)$; c and μ_0 are the speed of light and magnetic permeability in vacuum, respectively. Considering the incident light from air ($n_0 = 1$) onto WS_2, SiO_2, and Si, as illustrated in Figure 3, the whole optical transfer process of the trilayer system can be expressed by the transmission-matrix formalism[43] as follows:

$$M_{\text{substrate}} = M_{\text{Si}}M_{\text{SiO}_2}M_{\text{e}} \tag{4}$$

$$M_{\text{sample}} = M_{\text{Si}}M_{\text{SiO}_2}M_{\text{W}}M_{\text{e}} \tag{5}$$

where M_{Si}, M_{SiO_2}, and M_{W} represent the optical transfer properties of silicon, silicon oxide, and WS_2 layers, respectively. M_{e} represents the complex environmental influence surrounding the system. For simplicity, $M_{\text{e}} = I$ (unit matrix) considering the ideal circumstance. On the basis of eqs 2 and 3, the transfer matrix of WS_2 can be written as,

$$M_\omega = \begin{bmatrix} 1-\beta & -\beta \\ \beta & 1+\beta \end{bmatrix} \tag{6}$$

The reflected spectrum from the bare substrate can be deduced on the basis of eqs 4−6 and Fresnel's equations:[20]

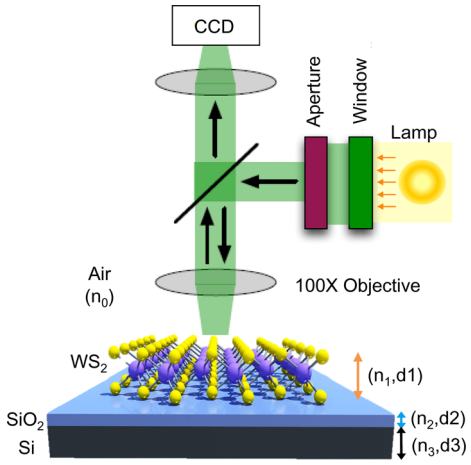

Figure 3. Schematic representation of the experimental setup used for reflection contrast spectroscopy. The white light is allowed to fall on the beam splitter after passing through an optical window and an aperture. The light is then reflected from a beam splitter to a 100× objective with numerical aperture NA = 0:95. By using an aperture stop, the illumination spot is reduced to ∼1 μm. When the light is incident on the $WS_2/SiO_2/Si$, it gets reflected and passes through beam splitter to either eye pieces or a CCD camera mounted on the microscope.

$$R_0 = |r_0|^2 = \left| \frac{r_{02} + r_{23} \times e^{-2i\phi_2}}{1 + r_{02} \times r_{23} \times e^{-2i\phi_2}} \right|^2 \quad (7)$$

Here, r_0 is the reflection coefficient of the air/SiO_2/Si interfaces; r_{02} and r_{23} are the individual reflection coefficients at the air/SiO_2 and SiO_2/Si interfaces, respectively. The phase difference when light passes through the SiO_2 layers is ϕ_2. The quantitative expressions for the above parameters are as follows; $r_{02} = (n_0 - n_2)/(n_0 + n_2)$, $r_{23} = (n_2 - n_3)/(n_2 + n_3)$, $\phi_2 = 2\pi n_2 d_2/\lambda$; n_0, n_2, and n_3 are the refractive indices of air, SiO_2, and Si, respectively; and d_2 is the thickness of the SiO_2 layer as shown in Figure 3. Similarly, the reflection spectrum of the WS_2 on SiO_2/Si can be calculated as,

$$R_W = \left| \frac{-r_0(1 - \beta) + \beta}{r_0\beta + (1 + \beta)} \right|^2 \quad (8)$$

By substituting the values of $n_0 = 1$, $n_2 = 1.47$, $n_3 = 3.42$, and $d_2 = 300$ nm in eq 7, the reflection spectrum R_0 is obtained, and subsequently, R_ω can be calculated as a function of optical conductivity $\sigma(\omega)$. Because the contrast spectrum R_ω of WS_2 layers can be obtained experimentally, the optical conductivity spectrum $\sigma(\omega)$ can be deduced by solving eqs 1 and 8.

Figure 4 presents the experimental reflection contrast spectra of the samples including monolayer, bilayer, multilayer, and bulk WS_2 in the visible to near-infrared region using eq 1. One can clearly see that there are obvious differences in the contrast peaks among the shown curves. A gradual and distinct red shift in contrast peaks are found to appear with increasing number of layers. For monolayer, the magnitude of the contrast is 5.4%, while that of bilayer, multilayer and bulk is found to be 14.3, 18.5 and 38.3%, respectively, as shown in Figure 4b. The higher contrast magnitude and peak broadening for bilayer, multilayer, and bulk flakes are the consequences of thicker WS_2 film.

The contrast peaks A and B observed at 630 nm (1.96 eV) and 548 nm (2.26 eV) for monolayer WS_2 correspond to the excitonic absorption, which arise from the direct gap transitions

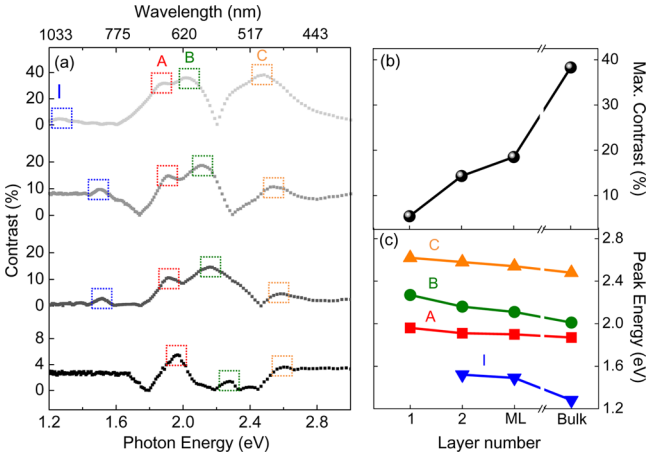

Figure 4. (a) Experimental reflection contrast spectra of as-prepared WS_2 flakes including monolayer to bulk form in the visible to near-infrared region using eq 1. The contrast peaks A, B, C, and I are labeled according to the convention proposed by Wilson and Yoffe.[7] (b) Maximum contrast % vs film thickness. (c) The positions of A, B, C, and I transitions as a function of film thickness in WS_2.

at the K point of the Brillouin zone. These observed peak positions match well with the PL peaks described in the previous section and also close to the values obtained from differential reflection spectra of layered WS_2 flakes.[5] The energy difference between the A and B peaks, (∼300 meV), is the measure of spin−orbital coupling strength and is a one-to-one correspondence with PL analysis. The contrast spectra show an additional peak at ∼2.62 eV for monolayer, labeled as C. Such a peak arises from one of the optical transitions between the density of states peaks in the valence and conduction bands.[5,44] Besides A, B, and C peaks, the contrast peak labeled as I in the near-infrared region corresponds to the indirect band gap transition for bilayer to bulk samples. The variation of A, B, C and I transition peaks as a function of layer number is plotted in Figure 4c. The I peak is absent in monolayer region, indicating that monolayer is a direct band gap semiconductor. Although multiple peaks are found to be present in near-infrared region, but these are close to noise level due to the low contrast signal.

The real part of the optical conductivity $\sigma_R(\omega)$ has been calculated by solving the eqs 1, 7, and 8 and is plotted in the energy range from 1.2 to 2.3 eV in Figure 5. It should be noted that $\sigma_R(\omega)$ is frequency dependent and behaves differently with number of layers. Optical conductivity spectra exhibit peaks at A, B, and I, and these peaks are shifted toward lower energy (Figure 5b) with increasing number of layers, which appears to mimic of contrast spectra. The exitonic transition peaks A and B observed at 1.96 and 2.25 eV for monolayer WS_2 with maximum magnitude of 0.37 $e^2/\pi\hbar$ reflect the ideal characteristics of direct band gap semiconductor, and this value is less than monolayer graphene (1.1 $e^2/\pi\hbar$)[38] in this energy range of the visible spectrum. A similar exitonic transition peak A in the photoconductivity spectrum has been observed for monolayer MoS_2 at 1.88 eV.[9] Nevertheless, the $\sigma_R(\omega)$ value reduces to 0.26 $e^2/\pi\hbar$ for 2L at peak A. This is obvious with a decrease in peak A and an increase in peak B with increasing number of layers. It can be noted that the magnitude of $\sigma_R(\omega)$ at the direct gap transitions A and B, which arises from the spin split valence bands and the conduction band at the K points, varies due to interlayer hopping for higher thickness. The large optical response and the peaks in the optical conductivity spectra as

dx.doi.org/10.1021/am5039483 | ACS Appl. Mater. Interfaces 2014, 6, 16020−16026

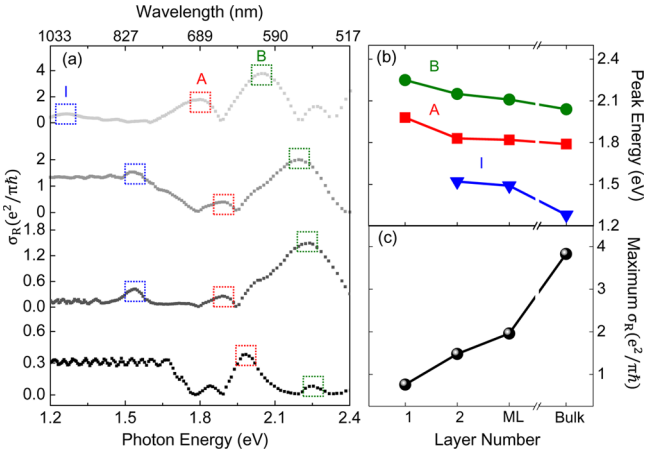

Figure 5. (a) Calculated real part of optical conductivity $\sigma_R(\omega)$ using eqs 1, 7, and 8 in the energy range 1.2−2.4 eV. The direct gap transitions at peaks A and B along with indirect gap transition at peak I are labeled. (b) The positions of $\sigma_R(\omega)$ transition peaks as a function of film thickness. (c) Maximum magnitude of $\sigma_R(\omega)$ vs film thickness in WS_2.

mentioned above are the consequences of band nesting in the large regions of the Brillouin zone for two-dimensional TMDCs recently reported by Carvalho et al.[22] The band nesting in two-dimensional materials results in a divergence of the joint density of states leading to high optical conductivity.

The indirect band gap transition peak I in the photoconductivity spectra is absent in monolayer WS_2. To confirm it, we have calculated the first-order derivative of the optical conductance for monolayer WS_2 (Figure S4, Supporting Information) and found that the region of 1.2−1.7 eV is almost flat, where a peak is expected. Fluctuations of the $d\sigma_R/dE$ in this region are attributed to noise, and this type of behavior has also been observed in the photoconductivity measurement on MoS_2.[9] The amplitude of the optical conductivity increases as the number of layers increases (Figure 5c) due to large density of states similar to MoS_2.[9] The above observations revel that the electronic structure of WS_2 is modified with evolution of number of layers, that is, transition from direct band gap (monolayer) toward indirect band gap (two or more layers), consistent with the theoretical prediction.[11]

2.5. Electronic Band Structure. The unit cell and first Brillouin zone of a monolayer WS_2 is displayed in Figure 6a,b. The electronic band structure was calculated using density functional theory (DFT) with details shown in Figure S3 (Supporting Information). The relevant structural parameters of WS_2 are taken from Ramasubramanian et al.[11]

Figure 6c,d show the electronic band structure of monolayer and five-layer WS_2, respectively, and that for bilayer and trilayer are provided in the Supporting Information. The direct band gap originates from the transition between the conduction band minimum and the valence band maximum at the high symmetry K point marked by a straight arrow for monolayer film. As the number of layers increases, the band gap turns to an indirect one that originates from the transition between the top of the valence band situated at Γ to the bottom of the conduction band halfway between Γ and K points marked by bend arrows for bilayer to multilayer samples. At the same time, the optical direct gap (at the K point) stays almost unchanged (independent of film thickness). This indirect to direct band gap transition from bulk or multilayer to monolayer WS_2 arises from quantum confinement effects.[11]

It is observed that the valence band edge at K splits into two, three, and five for bi-, tri-, and five-layer layer WS_2, respectively, due to interlayer hopping.[32] However, when the spin−orbital interaction is considered, the splitting pattern is completely changed, as recently reported by Zeng et al.[32] The valence band edge splits into two degenerate manifolds with a splitting magnitude (~0.4 eV) independent of the film thickness.

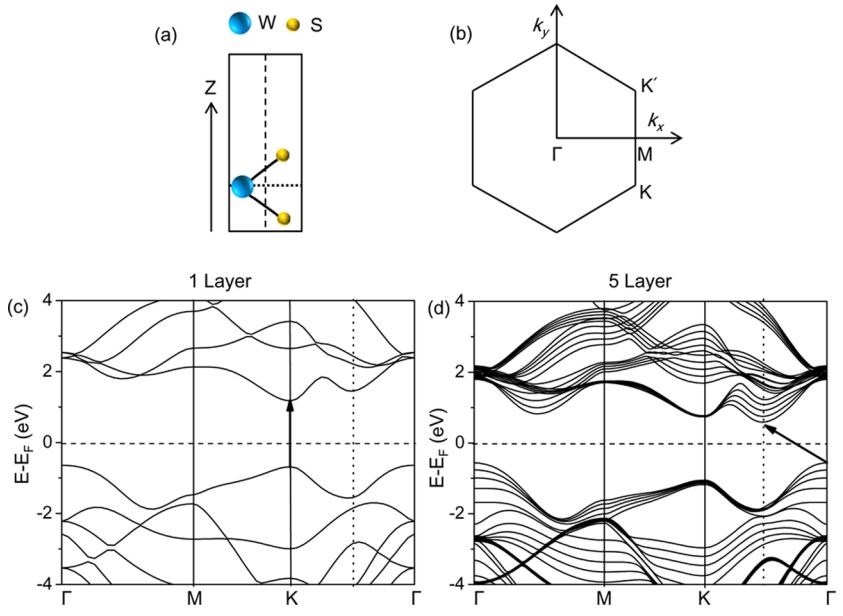

Figure 6. (a) 3D view of the 1H−WS_2 unit cell, containing one WS_2 layer. (b) First Brillouin zone of the WS_2 monolayer. Electronic band structures of (c) monolayer and (d) five-layer WS_2 using DFT. For five layers, the valence band splits into five degenerate states at K point due to interlayer hopping.

dx.doi.org/10.1021/am5039483 | ACS Appl. Mater. Interfaces 2014, 6, 16020−16026

3. CONCLUSIONS

In summary, we have investigated the optical conductivity of WS_2 platelets in the visible to near-infrared regions of the energy spectrum using reflection contrast spectroscopy. It is found that $\sigma(\omega)$ is frequency-dependent, in contrast to frequency-independent monolayer graphene in this energy range. For monolayer WS_2, the magnitude of optical conductivity at direct excitonic transition point K of the Brillouin zone is found to be 0.37 $e^2/\pi\hbar$ in the visible energy spectrum. Bilayer to bulk WS_2 samples show additional features in their conductivity spectra, signifying transition from direct band gap in monolayer to indirect band gap in two or more layers, as predicted by our calculations. This interesting optical conductivity behavior opens up the possibility to exciting opportunities of this material for fundamental research as well as for applications in photonics and optoelectronics. Additionally, the fact that this material can be synthesized directly on SiO_2/Si substrates using a simple method also opens up the possibility for two-dimensional device fabrications.

4. EXPERIMENTAL METHODS

4.1. Growth of WS_2. First, 300 nm SiO_2/Si substrates were cleaned with acetone, isopropyl alcohol, and standard SC-1 in a cleaning process in an ultrasonic bath for 10 min, and then they were dried with ultrahigh purity N_2 gas. These wafers were loaded into a physical vapor deposition chamber, and WO_3 was thermally evaporated and deposited on them with various thicknesses in the range of 10−25 nm. The thermal evaporation was carried out in a high vacuum (10^{-5}−10^{-6} Torr). Subsequently, the films were transferred into a quartz tube reactor for sulfurization. During the sulphurization of WO_3 films, a boat with 0.3 g of S powder (99.9% purity, Alfa Aesar) was kept upstream inside the quartz tube but outside the furnace. This zone was wrapped with an independently controlled thermal-coil, which was heated to a temperature ∼220 °C, as shown in Figure S5 (Supporting Information). The WO_3 films were heated to 850 °C for 30 min under Ar flow of 100 sccm and a slight hydrogen treatment below 10 sccm at low pressure (30 Torr), and they were reacted with S vapor to form WS_2 platelets, where the reactive zone is allowed at the temperature gradient region around 650−800 °C to synthesize high quality WS_2.

4.2. Characterization. The surface morphology of prepared WS_2 films was characterized by field emission scanning electron microscopy (FE-SEM, JEOL, JSM-700F). Layer thickness was measured by atomic force microscope using noncontact mode. Raman and PL spectroscopic studies were performed with a high-resolution MicroRaman spectrometer (LabRaman 800, Horiba Jobin Yvon) using a 514.5 nm (green line) laser source as the excitation wavelength. The spectra were collected in a backscattering geometry. Prior to taking measurements, we calibrated the system using 520.6 cm^{-1} phonon mode with a silicon substrate as reference. During the measurement, the sample was moved in the x−y direction under normal incidence.

4.3. Reflection Contrast Spectroscopy. The reflection contrast spectroscopy measurement was performed on WS_2 films directly deposited on silicon in the visible to near-infrared region (380−1100 nm) using a halogen lamp (model LE.5210−110, Euromex Iluminator EK-1, Holland) as a white light source equipped with an optical microscope (Olympus, model no. BX51RF). Both scattered light and reflected light were collected in a backscattering configuration, using an objective lens with a magnification of 100× and a numerical aperture (NA) of 0.95. The white light spot size was about 1 μm.

■ ASSOCIATED CONTENT

Ⓢ Supporting Information

Additional characterizations, band structure calculation using DFT, and experimental setup for WS_2 growth are provided in the Supporting Information. This material is available free of charge via the Internet at http://pubs.acs.org.

■ AUTHOR INFORMATION

Corresponding Author

*E-mail: pwchiu@ee.nthu.edu.tw.

Notes

The authors declare no competing financial interest.

■ ACKNOWLEDGMENTS

The authors acknowledge the support from the NTHU booster project and Taiwan National Science Council under contract no. NSC 100-2112-M-007-014-MY3.

■ REFERENCES

(1) Butler, S. Z.; Hollen, S. M.; Cao, L. Y.; Cui, Y.; Gupta, J. A.; Gutierrez, H. R.; Heinz, T. F.; Hong, S. S.; Huang, J. X.; Ismach, A. F.; Johnston-Halperin, E.; Kuno, M.; Plashnitsa, V. V.; Robinson, R. D.; Ruoff, R. S.; Salahuddin, S.; Shan, J.; Shi, L.; Spencer, M. G.; Terrones, M.; Windl, W.; Goldberger, J. E. Progress, Challenges, and Opportunities in Two-Dimensional Materials Beyond Graphene. *ACS Nano* **2013**, *7*, 2898−2926.

(2) Xu, M. S.; Liang, T.; Shi, M. M.; Chen, H. Z. Graphene-Like Two-Dimensional Materials. *Chem. Rev.* **2013**, *113*, 3766−3798.

(3) Perkins, F. K.; Friedman, A. L.; Cobas, E.; Campbell, P. M.; Jernigan, G. G.; Jonker, B. T. Chemical Vapor Sensing with Monolayer MoS_2. *Nano Lett.* **2013**, *13*, 668−673.

(4) Chen, W.; Santos, E. J. G.; Zhu, W. G.; Kaxiras, E.; Zhang, Z. Y. Tuning the Electronic and Chemical Properties of Monolayer MoS_2 Adsorbed on Transition Metal Substrates. *Nano Lett.* **2013**, *13*, 509−514.

(5) Zhao, W. J.; Ghorannevis, Z.; Chu, L. Q.; Toh, M. L.; Kloc, C.; Tan, P. H.; Eda, G. Evolution of Electronic Structure in Atomically Thin Sheets of WS_2 and WSe_2. *ACS Nano* **2013**, *7*, 791−797.

(6) Sahoo, S.; Gaur, A. P. S.; Ahmadi, M.; Guinel, M. J. F.; Katiyar, R. S. Temperature-Dependent Raman Studies and Thermal Conductivity of Few-Layer MoS_2. *J. Phys. Chem. C* **2013**, *117*, 9042−9047.

(7) Wilson, J. A.; Yoffe, A. D. Transition Metal Dichalcogenides Discussion and Interpretation of Observed Optical, Electrical, and Structural Properties. *Adv. Phys.* **1969**, *18*, 193−335.

(8) Yoffe, A. D. Layer Compounds. *Annu. Rev. Mater. Sci.* **1973**, *3*, 147−170.

(9) Mak, K. F.; Lee, C.; Hone, J.; Shan, J.; Heinz, T. F. Atomically Thin MoS_2: A New Direct-Gap Semiconductor. *Phys. Rev. Lett.* **2010**, *105*, 136805.

(10) Kuc, A.; Zibouche, N.; Heine, T. Influence of Quantum Confinement on the Electronic Structure of the Transition Metal Sulfide TS_2. *Phys. Rev. B* **2011**, *83*, 245213.

(11) Ramasubramaniam, A. Large Excitonic Effects in Monolayers of Molybdenum and Tungsten Dichalcogenides. *Phys. Rev. B* **2012**, *86*, 115409.

(12) Zeng, H.; Dai, J.; Yao, W.; Xiao, D.; Cui, X. Valley Polarization in MoS_2 Monolayers by Optical Pumping. *Nat. Nanotechnol.* **2012**, *7*, 490−493.

(13) Mak, K. F.; He, K.; Shan, J.; Heinz, T. F. Control of Valley Polarization in Monolayer MoS_2 by Optical Helicity. *Nat. Nanotechnol.* **2012**, *7*, 494−498.

(14) Schutte, W. J.; Deboer, J. L.; Jellinek, F. Crystal Structures of Tungsten Disulfide and Diselenide. *J. Solid State Chem.* **1987**, *70*, 207−209.

(15) Frey, G. L.; Tenne, R.; Matthews, M. J.; Dresselhaus, M. S.; Dresselhaus, G. Optical Properties of MS_2 (M = Mo, W) Inorganic Fullerene-Like and Nanotube Material Optical Absorption and Resonance Raman Measurements. *J. Mater. Res.* **1998**, *13*, 2412−2417.

(16) Ballif, C.; Regula, M.; Schmid, P. E.; Remskar, M.; Sanjines, R.; Levy, F. Preparation and Characterization of Highly Oriented,

Photoconducting WS_2 Thin Films. *Appl. Phys. A: Mater. Sci. Process.* **1996**, *62*, 543−546.
(17) Ma, Y. D.; Dai, Y.; Guo, M.; Niu, C. W.; Lu, J. B.; Huang, B. B. Electronic and Magnetic Properties of Perfect, Vacancy-Doped, and Nonmetal Adsorbed $MoSe_2$, $MoTe_2$, and WS_2 Monolayers. *Phys. Chem. Chem. Phys.* **2011**, *13*, 15546−15553.
(18) Bonaccorso, F.; Sun, Z.; Hasan, T.; Ferrari, A. C. Graphene Photonics and Optoelectronics. *Nat. Photonics* **2010**, *4*, 611−622.
(19) Stauber, T.; Peres, N. M. R.; Geim, A. K. Optical Conductivity of Graphene in the Visible Region of the Spectrum. *Phys. Rev. B* **2008**, *78*, 085432.
(20) Wang, Y. Y.; Ni, Z. H.; Liu, L.; Liu, Y. H.; Cong, C. X.; Yu, T.; Wang, X. J.; Shen, D. Z.; Shen, Z. X. Stacking-Dependent Optical Conductivity of Bilayer Graphene. *ACS Nano* **2010**, *4*, 4074−4080.
(21) Gutiérrez, H. R.; Perea-López, N.; Elías, A. L.; Berkdemir, A.; Wang, B.; Lv, R.; López-Urías, F.; Crespi, V. H.; Terrones, H.; Terrones, M. Extraordinary Room-Temperature Photoluminescence in Triangular WS_2 Monolayers. *Nano Lett.* **2013**, *13*, 3447−3454.
(22) Carvalho, A.; Ribeiro, R. M.; Neto, A. H. C. Band Nesting and the Optical Response of Two-Dimensional Semiconducting Transition Metal Dichalcogenides. *Phys. Rev. B* **2013**, *88*, 115205.
(23) Thripuranthaka, M.; Late, D. J. Temperature Dependent Phonon Shifts in Single-Layer WS_2. *ACS Appl. Mater. Interfaces* **2014**, *6*, 1158−1163.
(24) Ferrari, A. C.; Meyer, J. C.; Scardaci, V.; Casiraghi, C.; Lazzeri, M.; Mauri, F.; Piscanec, S.; Jiang, D.; Novoselov, K. S.; Roth, S.; Geim, A. K. Raman Spectrum of Graphene and Graphene Layers. *Phys. Rev. Lett.* **2006**, *97*, 187401.
(25) Lee, C.; Yan, H.; Brus, L. E.; Heinz, T. F.; Hone, J.; Ryu, S. Anomalous Lattice Vibrations of Single- and Few-Layer MoS_2. *ACS Nano* **2010**, *4*, 2695−2700.
(26) Najmaei, S.; Liu, Z.; Ajayan, P. M.; Lou, J. Thermal Effects on the Characteristic Raman Spectrum of Molybdenum Disulfide (MoS_2) of Varying Thicknesses. *Appl. Phys. Lett.* **2012**, *100*, 013106.
(27) Berkdemir, A.; Gutiérrez, H. R.; Botello-Mendez, A. R.; Perea-López, N.; Elías, A. L.; Chia, C. I.; Wang, B.; Crespi, V. H.; López-Urías, F.; Charlier, J. C.; Terrones, H.; Terrones, M. Identification of Individual and Few Layers of WS_2 Using Raman Spectroscopy. *Sci. Rep.* **2013**, *3*, 1755.
(28) Ramakrishna Matte, H. S. S.; Gomathi, A.; Manna, A. K.; Late, D. J.; Datta, R.; Pati, S. K.; Rao, C. N. R. MoS_2 and WS_2 Analogues of Graphene. *Angew. Chem., Int. Ed.* **2010**, *49*, 4059−4062.
(29) Zhang, X.; Han, W. P.; Wu, J. B.; Milana, S.; Lu, Y.; Li, Q. Q.; Ferrari, A. C.; Tan, P. H. Raman Spectroscopy of Shear and Layer Breathing Modes in Multilayer MoS_2. *Phys. Rev. B* **2013**, *87*, 115413.
(30) Molina-Sánchez, A.; Wirtz, L. Phonons in Single-Layer and Few-Layer MoS_2 and WS_2. *Phys. Rev. B* **2011**, *84*, 155413.
(31) Wang, Q. H.; Kalantar-Zadeh, K.; Kis, A.; Coleman, J. N.; Strano, M. S. Electronics and Optoelectronics of Two-Dimensional Transition Metal Dichalcogenides. *Nat. Nanotechnol.* **2012**, *7*, 699−712.
(32) Zeng, H. L.; Liu, G. B.; Dai, J. F.; Yan, Y. J.; Zhu, B. R.; He, R. C.; Xie, L.; Xu, S. J.; Chen, X. H.; Yao, W.; Cui, X. D. Optical Signature of Symmetry Variations and Spin-Valley Coupling in Atomically Thin Tungsten Dichalcogenides. *Sci. Rep.* **2013**, *3*, 1608.
(33) Cheiwchanchamnangij, T.; Lambrecht, W. R. L. Quasiparticle Band Structure Calculation of Monolayer, Bilayer, and Bulk MoS_2. *Phys. Rev. B* **2012**, *85*, 205302.
(34) Zhang, Y.; Zhang, Y. F.; Ji, Q. Q.; Ju, J.; Yuan, H. T.; Shi, J. P.; Gao, T.; Ma, D. L.; Liu, M. X.; Chen, Y. B.; Song, X. J.; Hwang, H. Y.; Cui, Y.; Liu, Z. F. Controlled Growth of High-Quality Monolayer WS_2 Layers on Sapphire and Imaging Its Grain Boundary. *ACS Nano* **2013**, *7*, 8963−8971.
(35) Yun, W. S.; Han, S. W.; Hong, S. C.; Kim, I. G.; Lee, J. D. Thickness and Strain Effects on Electronic Structures of Transition Metal Dichalcogenides: 2H-MX_2 semiconductors (M = Mo, W; X = S, Se, Te). *Phys. Rev. B* **2012**, *85*, 033305.
(36) Jiang, H. Electronic Band Structures of Molybdenum and Tungsten Dichalcogenides by the GW Approach. *J. Phys. Chem. C* **2012**, *116*, 7664−7671.
(37) Ni, Z. H.; Wang, H. M.; Kasim, J.; Fan, H. M.; Yu, T.; Wu, Y. H.; Feng, Y. P.; Shen, Z. X. Graphene Thickness Determination Using Reflection and Contrast Spectroscopy. *Nano Lett.* **2007**, *7*, 2758−2763.
(38) Fei, Z.; Shi, Y.; Pu, L.; Gao, F.; Liu, Y.; Sheng, L.; Wang, B. G.; Zhang, R.; Zheng, Y. D. High-Energy Optical Conductivity of Graphene Determined by Reflection Contrast Spectroscopy. *Phys. Rev. B* **2008**, *78*, 201402.
(39) Nair, R. R.; Blake, P.; Grigorenko, A. N.; Novoselov, K. S.; Booth, T. J.; Stauber, T.; Peres, N. M. R.; Geim, A. K. Fine Structure Constant Defines Visual Transparency of Graphene. *Science* **2008**, *320*, 1308−1308.
(40) Du, C. L.; You, Y. M.; Kasim, J.; Ni, Z. H.; Yu, T.; Wong, C. P.; Fan, H. M.; Shen, Z. X. Confocal White Light Reflection Imaging for Characterization of Metal Nanostructures. *Opt. Commun.* **2008**, *281*, 5360−5363.
(41) Teo, G. Q.; Wang, H. M.; Wu, Y. H.; Guo, Z. B.; Zhang, J.; Ni, Z. H.; Shen, Z. X. Visibility Study of Graphene Multilayer Structures. *J. Appl. Phys.* **2008**, *103*, 124302.
(42) Kuzmenko, A. B.; van Heumen, E.; Carbone, F.; van der Marel, D. Universal Optical Conductance of Graphite. *Phys. Rev. Lett.* **2008**, *100*, 117401.
(43) Roddaro, S.; Pingue, P.; Piazza, V.; Pellegrini, V.; Beltram, F. The Optical Visibility of Graphene: Interference Colors of Ultrathin Graphite on SiO_2. *Nano Lett.* **2007**, *7*, 2707−2710.
(44) Mattheiss, L. F. Band Structures of Transition-Metal-Dichalcogenide Layer Compounds. *Phys. Rev. B* **1973**, *8*, 3719−3740.